Modeling Convective Heat Transfer Augmentation of TiO_2 Nanofluids using Neural Networks

Zeinab pouramini

Abstract

In this research, a neural network methodology was implemented to predict the forced convective heat transfer coefficient of nanofluids. Various solutions with distinct TiO2 nanoparticle concentrations were synthesized through the two-step method and directed upward within a vertical pipe under both laminar and turbulent flow conditions. The investigation covered diverse operational parameters, including heat flux, thermal conductivity of fluids, nanoparticle concentration, and flow Reynolds number, to quantify the convective heat transfer coefficient. These operational parameters were incorporated as inputs into an artificial neural network to model the convective heat transfer coefficient. Evaluation metrics, such as mean square error and correlation coefficient, were computed, revealing the remarkable performance of the neural network in capturing the underlying processes. The introduction of nanoparticles into the base fluid significantly amplified the forced convective heat transfer coefficient, with more pronounced effects observed in base fluids exhibiting lower thermal conductivity and flows characterized by higher Reynolds numbers and elevated heat fluxes. The findings underscore the efficacy of neural networks in elucidating the complex interactions governing convective heat transfer in nanofluids.

1 Introduction

Improving the efficiency of working fluids in thermo systems enhances their overall performance and minimizes size requirements. Nanofluids, which are suspensions of small percentages (¡5 vol. %) of various nanoparticles in conventional working fluids, have emerged as an excellent solution to address the thermal challenges in advanced heat transfer systems.

In a study by Pak and Cho on nanofluids consisting of 3 vol. % 27 nm titanium dioxide particles in water, a new correlation for turbulent convective heat transfer in dilute nanofluids was reported [1]:

$$\mathbf{Nu} = 0.21\mathbf{Re}^{0.8}\mathbf{Pr}^{0.5} \tag{1}$$

where **Nu** is the Nusselt number, **Re** is the Reynolds number, and **Pr** is the Prandtl number and $6.54 \leq \mathrm{Pr} \leq 12.33, \quad 10^4 \leq \mathrm{Re} \leq 10^5$

He et al. synthesized stable aqueous 20 nm titanium dioxide nanofluids with different agglomerate sizes and concentrations, revealing an increase in convective heat transfer coefficient with nanoparticle concentration, particularly in turbulent flow regimes [2].

2 Related Works

While experimental studies provide valuable insights, more research is needed to model the intricate processes and establish empirical relations between effective parameters. Artificial neural networks (ANNs) have proven effective in modeling various processes. For instance, Santra et al. applied ANN to predict heat transfer in laminar natural convection of copper–water nanofluids, demonstrating accurate predictions within the training data range [3]. Fazeli et al. utilized ANN to simulate the heat transfer characteristics of a miniature heat sink cooled by SiO2–water nanofluids, achieving excellent agreement with mathematical simulations [4]. Balcilar et al. employed ANNs to determine parameters' effects on the heat transfer coefficient of nanofluids, showing good

agreement with experimental data [5].

Papari et al. utilized ANN analysis to estimate the thermal conductivity of nanofluids containing multi-walled carbon nanotubes (MWCNTs) and single-walled carbon nanotubes (SWCNTs), with predicted values in good agreement with literature [6]. Hojjat et al. synthesized various nanofluids and proposed neural network models to represent thermal conductivity as a function of temperature, nanoparticle concentration, and the thermal conductivity of nanoparticles [7].

In this paper, we employ neural networks to estimate the forced convective heat transfer coefficient of nanofluids. The study aims to compare the modeling results with experimental data obtained for water and an ethylene glycol/water mixture as the base fluid. Nanofluids containing TiO2 nanoparticles at various concentrations will be tested under different heat flux boundary conditions, flowing upward through a vertical pipe in laminar and turbulent flow regimes.

3 Experimental Setup

Spherical titanium dioxide nanoparticles dispersed in distilled water and ethylene glycol/water mixture (60 weight-% ethylene glycol) were used. Nanoparticles were purchased from Degussa (Germany) with an average diameter of 25 nm. An ultrasonic vibrator (Tecna 6) was used for the preparation of mixed aqueous suspensions. The suspension was sonicated for 4 hours at a frequency of 50-60 kHz with an output power of 138W, at 65^{o}C, and pH=11 by NaOH solution. Nanofluids containing 0.5%, 1.0%, 1.5% titanium dioxide by volume were obtained using the two-step method. The stability time of nanofluids was observed to be 24 hours without any stabilizer.

The test section in Fig. 1 (experimental apparatus) was a straight copper tube with a length of 120 cm, an inner diameter of 6 mm, and an outer diameter of 8 mm. Two rods of heaters with different AC power in parallel with the tube were used as heaters with a thick thermal isolating layer. Four (K-type) thermocouples were welded on the inner tube wall at 20 cm (Tw1), 50 cm (Tw2),

80 cm (Tw3), and 110 cm (Tw4) from the inlet of the test section. Two further K-type thermocouples were inserted into the flow at 8 cm (Tfin) and 119 cm (Tfout) from the inlet of the test section. After injection of nanofluid into a glass vessel as a fluid reservoir tank, it was circulated toward the test section using a pump (STAR RS 25/6-130). Flow rate was measured by a flow meter, and different flow rates (0.5-5.0 L/min) were obtained by using a valve before the flow meter. To cool nanofluids, a tube-in-shell type heat exchanger was used.

3.1 Problem Formulation

The experimental data served as the basis for calculating the convective heat transfer coefficient (h) and Nusselt number (Nu) using the following equations:

$$q = h \cdot (T_w - T_f) \quad (2) \tag{2}$$

where q is the heat flux, T_w is the measured wall temperature, and T_f is the fluid temperature calculated through the energy balance equation:

$$q = \rho_f \cdot c_f \cdot Q \cdot (T_{\text{fin}} - T_f) \quad (3) \tag{3}$$

Here, T_{fin} is the measured fluid temperature at the inlet of the test section, c_f is the fluid heat capacity, ρ_f is the fluid density, S is the perimeter of the test tube, and Q is the flow rate. For nanofluids, the value of ρc was calculated using the equation:

$$\rho c = \rho_f \cdot c_f + \rho_p \cdot c_p \cdot VF \quad (4) \tag{4}$$

Comparing the measured fluid temperature at the outlet of the test section with the theoretical value calculated by Eq. (3) revealed a maximum deviation lower than 12

The convective heat transfer coefficient, h, in Eq. (2), is often expressed in the form of the Nusselt number (Nu):

$$Nu = \frac{h \cdot D}{k_f} \quad (5) \tag{5}$$

Here, D is the tube inner diameter, and k_f is the fluid thermal conductivity. For nanofluids, k_f is predicted by the H-C model [8]:

$$k_f = k_f \cdot [1 + 2.5 \cdot \phi] \quad (6) \tag{6}$$

where ϕ is the volume fraction of nanoparticles. Additionally, the Nusselt number is traditionally related to the Reynolds number (Re) and the Prandtl number (Pr):

$$Nu = C \cdot Re^m \cdot Pr^n \quad (7) \tag{7}$$

where C, m, and n are constants. The Reynolds number (Re) and the Prandtl number (Pr) are defined as:

$$Re = \frac{\rho_f \cdot u \cdot D}{\mu_f} \quad (8) \tag{8}$$

$$Pr = \frac{\mu_f \cdot c_f}{k_f} \quad (9) \tag{9}$$

For nanofluids, the Prandtl number is predicted by the Einstein equation. In Eq. (7), x represents the axial distance from the entrance of the test section.

4 Modeling

In this study, an artificial neural network (ANN) program was developed using the MATLAB software environment. A total of 56 experimental datasets, derived from various experiments, were utilized to construct a three-layer feed-forward neural network model. The hyperbolic tangent sigmoid (`tansig`) transfer function with a back-propagation algorithm at the hidden layer and a linear transfer function (`purelin`) at the output layer were employed.

To enhance the numerical stability (accuracy index) of the model construction, both inputs and targets were initially normalized to produce data with zero mean and unity standard deviation. Principal component analysis (PCA) was then performed before the training stage. The number of principal components, accounting for 98% of the variation, equaled the number of original input parameters, indicating no redundancy in the dataset.

Next, the datasets were divided into three sets: a training dataset comprising one-half of the data for training the ANN, a validation dataset with one-quarter of the data for validating the developed ANN, and a testing set with one-quarter of the data for evaluating the ANN. Various learning algorithms were applied to select the best one, followed by optimization between the neuron number and mean squared error (MSE) for the chosen learning algorithm.

Different statistical parameters, such as mean absolute error (MAE), MSE, root mean squared error (RMSE), and determination coefficient (R^2), were calculated to assess the accuracy of the modeling process.

5 Results and Discussion

5.1 Learning Algorithm Selection

To identify the optimal back-propagation learning algorithm, various algorithms were employed. A three-layer feed-forward artificial neural network (ANN) with a hyperbolic tangent sigmoid (`tansig`) transfer function at the hidden layer and a linear (`purelin`) transfer function at the output layer was utilized for all back-propagation learning algorithms. Ten neurons were consistently used in the hidden layer for all algorithms. The results are summarized in Table 1.

Learning Algorithm	**Minimum MSE**
Levenberg–Marquardt (LM)	0.0010

Table 1: Performance comparison of back-propagation learning algorithms.

As evident from Table 1, the Levenberg–Marquardt (LM) algorithm exhib-

10ht]

Number of Neurons in Hidden Layer	MSE
2	0.0021
4	0.0015
6	0.0008
8	0.0013
9	0.0016

Table 2: Optimization of the number of neurons in the hidden layer.

ited the lowest Mean Squared Error (MSE) of 0.0010, establishing it as the most effective back-propagation learning algorithm.

5.2 Optimization of Artificial Neural Network

The number of hidden layer neurons significantly influences the performance of artificial neural networks (ANNs). Inappropriately low values hinder proper training, while excessively high values lead to overfitting [9]. The optimal number of neurons in the hidden layer was determined through trial and error, ranging from 2 to 9 neurons. The relationship between the number of hidden layer neurons and MSE is presented in Table 2. The minimum MSE value of 0.0008 was observed with 6 neurons in the hidden layer. Consequently, the ANN was configured with 6 neurons in the hidden layer.

5.3 Convective Heat Transfer Coefficient of Distilled Water

The experimental system was tested with distilled water at Reynolds numbers of 2960 and 3960. To validate the constant heat flux boundary condition, the experimental data of the convective heat transfer coefficient of distilled water, represented as the Nusselt number (Nu), was compared with the predicted Nu number from the Gnielinski equation [10]. The Gnielinski equation for constant heat flux boundary conditions is given by:

$$Nu = \left(0.155 \cdot Re^{0.33}\right) \cdot Pr^{0.33} \tag{10}$$

The experimental and predicted Nu numbers for Reynolds numbers 2960 and 3960 are shown in Figures 2(a) and 2(b). The Gnielinski equation predicts the experimental data with a 4 % deviation for $Re = 2960$ and a 3 % deviation for $Re = 3960$. These deviations are attributed to the influence of the entrance on the heat transfer coefficient, not accounted for in Eq. (10). Therefore, the constant heat flux boundary condition for this study is deemed valid.

5.4 Effect of Nanoparticle Concentrations on the Convective Heat Transfer Coefficient in Distilled Water

In Figures 3(a) and 3(b), the experimental results and predicted data from the ANN were compared. The axial profiles of the heat transfer coefficient of nanofluids show an increase with increasing particle concentration. The enhancement is more pronounced at higher Reynolds numbers. For instance, at $Re = 2960$ and $Re = 3960$, the maximum enhancement with 1.50 vol.% TiO_2 nanofluids is about 40% (see Fig. 3(a)) and more than 52% (see Fig. 3(b)), respectively. The good agreement between experimental results and predicted data demonstrates the high accuracy of the ANN in predicting this process.

5.5 Convective Heat Transfer Coefficient of Water/Ethylene Glycol Mixture

The experimental system was tested with a mixture consisting of 60 weight-% ethylene glycol and 40 weight-% distilled water at $Re = 2030$. Figure 4 shows the measured data, comparing it with calculated values from the Shah equation [11]. The Shah equation for laminar flows under constant heat flux boundary conditions is given by

$$Nu = \left(1.86 + \frac{0.86 \cdot Re^{0.5} \cdot Pr^{0.33}}{\left(1 + 0.12 \cdot (Re \cdot Pr)^{0.666}\right)^{0.25}}\right) \tag{11}$$

The Shah equation predicts the experimental data with a 1.5% deviation for $Re = 2030$.

5.6 Effect of Nanoparticle Concentration on the Convective Heat Transfer Coefficient in the Mixture of Water and Ethylene Glycol

Figure 5 shows the axial profiles of the convective heat transfer coefficient of nanofluids with different TiO_2 particle concentrations in the mixture consisting of 60 weight-% ethylene glycol and 40 weight-% distilled water at $Re = 2030$. The convective heat transfer coefficient was indicated based on experimental data and ANN results. This figure shows that with an increasing particle concentration, the convective heat transfer coefficient of TiO_2 increases.

5.7 Effect of Heat Flux on the Convective Heat Transfer Coefficient of Nanofluid

Figure 6 shows the enhancement of the convective heat transfer coefficient for power supplies of 440W and 550W based on experimental data and ANN results. In this figure, the convective heat transfer coefficient in distilled water nanofluid increases with an increasing heat flux. Results also show that the improvement of convective heat transfer coefficient of the base fluid due to the addition of nanoparticles seems to be more considerable in turbulent flow regimes and higher heat fluxes. Comparing experimental data and ANN results indicates that the ANN could predict this process better at lower heat flux than at higher heat flux.

6 Conclusions

In this study, experimental work has been conducted to investigate the heat transfer behavior of TiO_2 nanofluids flowing through a straight vertical pipe under both laminar and turbulent flow conditions. The obtained results were uti-

lized by an Artificial Neural Network (ANN) to model this process. The effects of operational parameters such as nanoparticle concentrations, flow Reynolds number, type of base fluid, and heat flux were investigated. The following conclusions can be drawn from the results of experiments in this study:

- Addition of nanoparticles into the base fluid enhances the convective heat transfer coefficient, and the enhancement increases with increasing particle concentration.
- The enhancement due to the addition of nanoparticles seems to be more considerable at higher Reynolds numbers.
- The convective heat transfer coefficient enhancement for the mixture consisting of 60 weight-% ethylene glycol and 40 weight-% distilled water is greater than the nanofluid of distilled water alone.
- The use of TiO_2 nanoparticles as the dispersed phase in distilled water can significantly enhance the convective heat transfer, and the enhancement increases with increasing heat flux.
- Good agreement between experimental data and predicted results of the ANN shows that the ANN can be used to model this process with high accuracy, except for higher heat flux.

References

[1] B.C. Pak and Y.I. Cho. Hydrodynamic and heat transfer study of dispersed fluids with submicron metallic oxide particle. *Exp. Heat Transfer*, 11:151–170, 1998.

[2] Y. He, Y. Men, Y. Zhao, H. Lu, and Y. Ding. Numerical investigation into the convective heat transfer of tio2 nanofluids flowing through a straight tube under the laminar flow conditions. *Appl. Therm. Eng.*, 29:1965–1972, 2009.

[3] A. K. Santra, N. Chakraborty, and S. Sen. Prediction of heat transfer due to presence of copper–water nanofluid using resilient-propagation neural network. *International Journal of Thermal Sciences*, 48:1311–1318, 2009.

[4] S. A. Fazeli, S. M. Hosseini Hashemi, H. Zirakzadeh, and Mehdi Ashjaee. Experimental and numerical investigation of heat transfer in a miniature heat sink utilizing silica nanofluid. *Superlattices and Microstructures*, 51:247–264, 2012.

[5] M. Balcilar, A.S. Dalkilic, A. Suriyawong, T. Yiamsawas, and S. Wongwises. Investigation of pool boiling of nanofluids using artificial neural networks and correlation development techniques. *International Communications in Heat and Mass Transfer*, 39:424–431, 2012.

[6] M. M. Papari, F. Yousefi, J. Moghadasi, H. Karimi, and A. Campo. Modeling thermal conductivity augmentation of nanofluids using diffusion neural networks. *International Journal of Thermal Sciences*, 50:44–52, 2011.

[7] M. Hojjat, S.Gh. Etemad, R. Bagheri, and J. Thibault. Thermal conductivity of non-newtonian nanofluids: Experimental data and modeling using neural network. *International Journal of Heat and Mass Transfer*, 54:1017–1023, 2011.

[8] R.L. Hamilton and O.K. Crosser. Thermal conductivity of heterogeneous two-component systems. *I & EC Fundam.*, 125 (3):187–191, 1962.

[9] A.B. Bulsari. *Neural networks for chemical engineers*. Elsevier Science Inc., New York, 1995.

[10] V. Gnielinski. New equations for heat and mass transfer in turbulent pipe and channel flow. *Int. Chem. Eng.*, 16:359–368, 1976.

[11] R. K Shah. Thermal entry length solutions for the circular tube and parallel plates. pages 11–75, 1975.

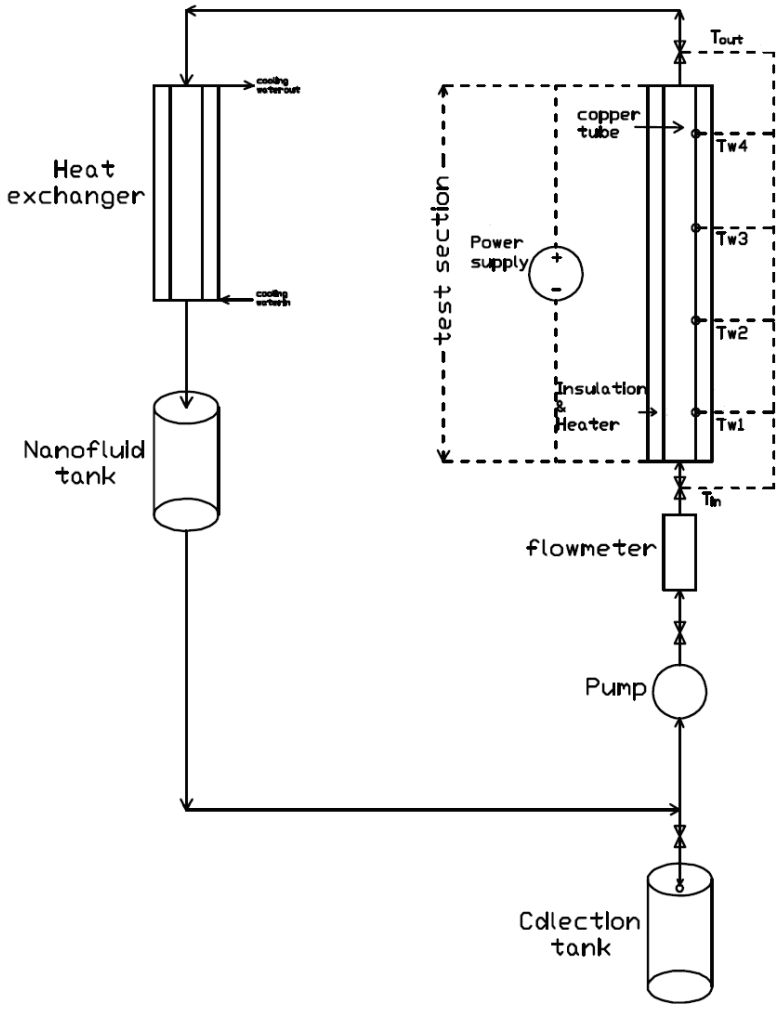
Heat
exchanger
Nanofluid
tank
test section
copper
tube
Power
supply
+
-
Insulation
&
Heater
Tout
Tw4
Tw3
Tw2
Tw1
Tin
flowmeter
Pump
Collection
tank

Figure 1:

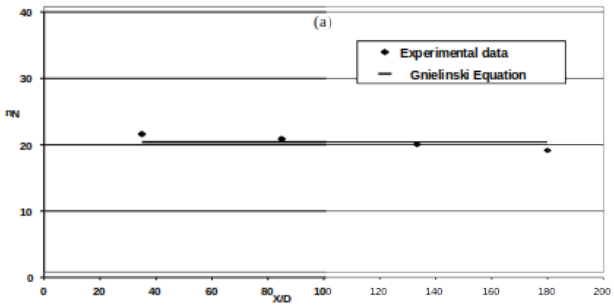

Figure 2:

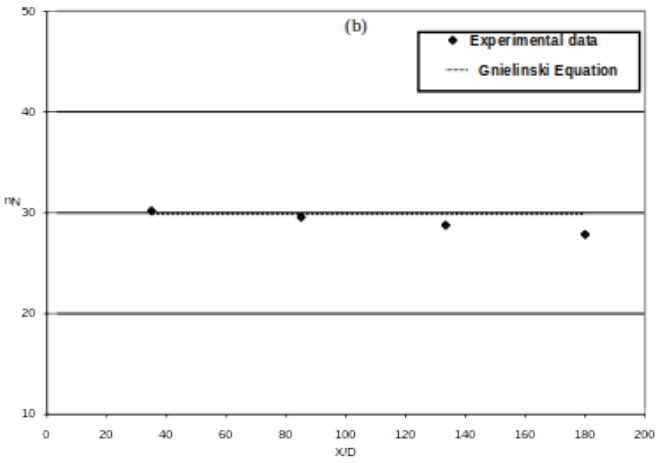

Figure 3:

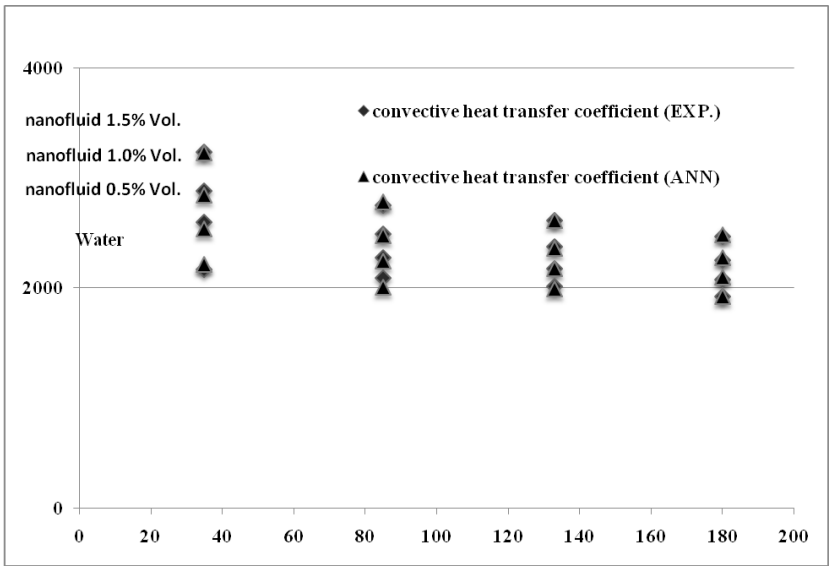

Figure 4:

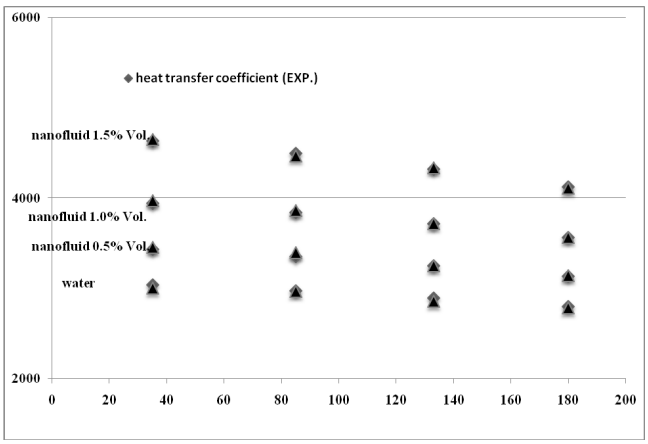

Figure 5:

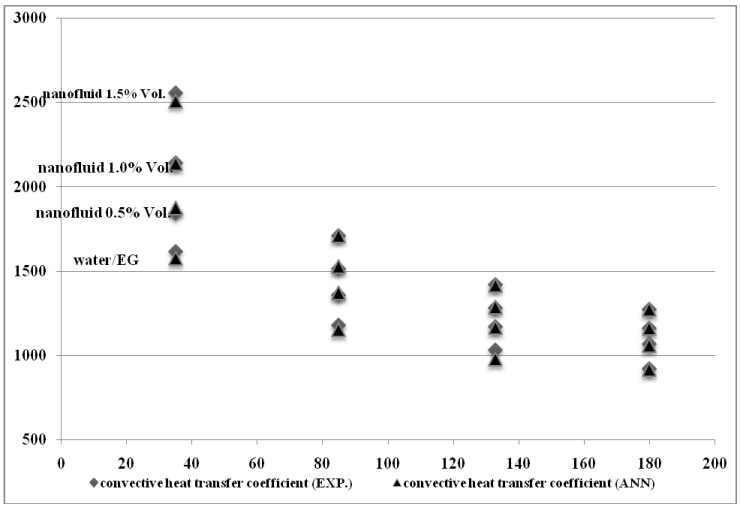

Figure 6:

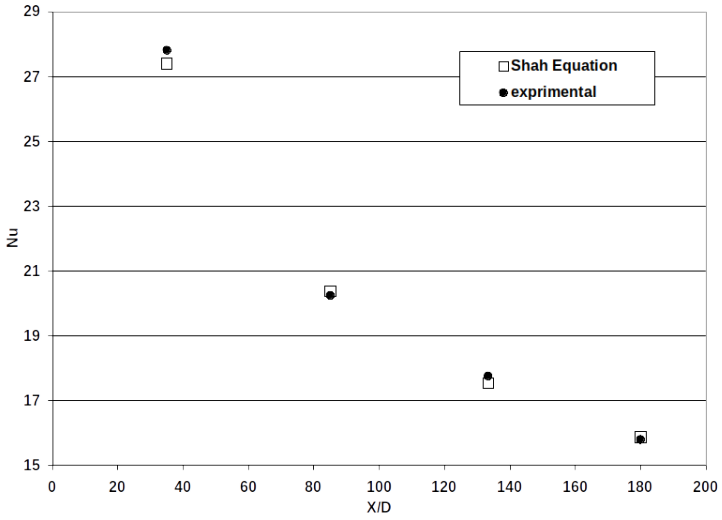

Figure 7:

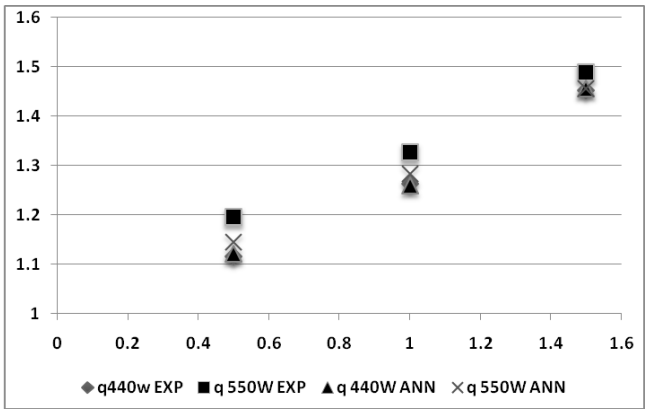

Figure 8:

Table 3: Comparison of various back propagation learning algorithms

R2	MSE	Function	Back Propagation Algorithm
0.9899	0.0099	trainrp	Resilient backpropagation (Rprop)
0.9969	0.0031	traincgf	Fletcher–Reeves conjugate gradient backpropagation
0.9957	0.0042	traincgp	Polak–Ribi´ere conjugate gradient backpropagation
0.9960	0.0039	traincgb	Powell–Beale conjugate gradient backpropagation
0.9990	0.0010	trainlm	Levenberg–Marquardt backpropagation
0.9944	0.0112	trainscg	Scaled conjugate gradient backpropagation
0.9963	0.0037	trainbfg	BFGS quasi-Newton backpropagation
0.9957	0.0042	trainoss	One step secant backpropagation
0.9910	0.0089	traingd	Batch gradient descent
0.7778	0.2186	traingdx	Variable learning rate backpropagation
0.8963	0.1061	traingdm	Batch gradient descent with momentum

Table 4: Number of neurons in hidden layer with related mean square errors.

MSE $\times 10^2$	Number of Neurons
1.69	2
0.31	3
0.23	4
0.17	5
0.08	6
0.20	7
0.11	8
0.15	9